Wadi Alshatti University Journal of Pure and Applied Sciences

مجلة جامعة وادي الشاطئ للعلوم البحتة و التطبيقية

Volume 4, No. 2, July-December 2026 Online ISSN: 3006-0877 المجلد 4، الاصدار 2، يوليو - ديسمبر 2026

RESEARCH ARTICLE ELECTRICAL AND ELECTRONIC ENGINEERING

Comparison of R-Adaptive Unscented Kalman Filters for Sensorless PMSM Estimation

Salah G. Abokhatwa[1,*], Abubaker Omran Zawam[2]

[1]Department of Electrical and Computer Engineering, Faculty of Engineering, El Mergib University, Al Khums, Libya
[2]Department of Electrical and Electronic Engineering, Higher Institute of Science and Technology, Qasr Ben Ghashir, Libya

ARTICLE HISTORY

Received 02 August 2026
Revised 09 September 2026
Accepted 15 September 2026
Online 18 September 2026

KEYWORDS

Permanent magnet synchronous motor;
Sensorless state estimation;
Adaptive unscented Kalman filter;
Measurement-noise covariance;
Statistical consistency;
Monte Carlo simulation.

ABSTRACT

This paper compares three unscented Kalman filters that adapt the measurement covariance R for sensorless permanent magnet synchronous motor (PMSM) estimation: an exponentially weighted UKF (UKF-QR), a master–slave UKF (UKF-MSQ), and a bounded Sage–Husa UKF (UKF-SH). The main contribution is a controlled comparison using the same initial conditions, voltage inputs, and noisy current measurements along a common PMSM trajectory generated by linear quadratic integral (LQI) speed control. Each adaptation coefficient is selected independently using Bayesian optimization and development tests, then fixed before evaluation. Two 50-trial Monte Carlo tests examine measurement-noise changes alone and in combination with parameter mismatch, speed changes, and load disturbances. Fixed-R and oracle-R UKFs provide reference results. In the noise-only test, the adaptive filters reduce settled-window mean squared error (MSE) by about 80% for d-axis current, 86% for q-axis current, and 70–71% for speed relative to the fixed UKF. UKF-QR gives the lowest MSE among the adaptive filters. Under combined stress, UKF-MSQ gives the lowest adaptive d-axis current and speed MSE, 2.809 × 10^{-3} A^2 and 7.265 × 10^{-3} (rad/s)^2, and the best average covariance tracking. UKF-QR gives the lowest adaptive q-axis current MSE. UKF-MSQ also has the lowest 95th-percentile speed MSE among the adaptive filters, although the fixed and oracle-R references give lower values. These results favor UKF-MSQ when average speed accuracy and covariance tracking are the main priorities under the tested disturbances.

مقارنة مرشحات UKF المتكيفة مع تغاير القياس لتقدير حالات المحرك المتزامن ذي المغناطيس الدائم دون مستشعرات

صلاح جمعه ابوخطوه[1,*] ، ابوبكر عمران الزوام[2]

الملخص

تقارن هذه الدراسة بين ثلاثة مرشحات UKF تتكيف مع مصفوفة تغاير القياس R لتقدير حالات المحرك المتزامن ذي المغناطيس الدائم (PMSM) دون مستشعرات، وهي المرشح ذو الترجيح الأسي (QR-UKF)، ومرشح السيد والتابع (UKF-MSQ)، ومرشح Sage–Husa المقيد (SH-UKF). تتمثل المساهمة الرئيسة في إجراء مقارنة تستخدم الظروف الابتدائية نفسها، ومدخلات الجهد نفسها، وقياسات التيار المشوشة نفسها، على مسار تشغيل مشترك يولده متحكم خطي تربيعي تكاملي (LQI) للسرعة. ويُختار معامل التكيف لكل مرشح بصورة مستقلة باستخدام خوارزمية تحسين بايزية واختبارات تطويرية، ثم يُثبت قبل التقييم. أُجري اختباران بطريقة مونت كارلو، يتكون كل منهما من 50 تجربة؛ يتناول الأول تغير ضوضاء القياس فقط، بينما يجمع الثاني بين تغير الضوضاء وعدم تطابق معاملات المحرك وتغيرات السرعة واضطرابات الحمل. واستُخدم مرشح ثابت التغاير وآخر يعتمد التغاير الحقيقي للقياس (R-oracle) مرجعين للمقارنة. في اختبار الضوضاء فقط، خفضت المرشحات المتكيفة متوسط مربع الخطأ (MSE) في فترات الاستقرار بنحو 80% لتيار المحور d، و86% لتيار المحور q، و70%-71% للسرعة مقارنة بالمرشح الثابت، وسجل QR-UKF أدنى القيم بين المرشحات المتكيفة. وفي الاختبار المركب، حقق MSQ-UKF أدنى متوسط لمربع الخطأ بين المرشحات المتكيفة لتيار المحور d والسرعة، بقيمتي 2.809 × 10^{-3} A^2 و 7.265 × 10^{-3} (rad/s)^2، وأفضل متوسط لدقة تتبع التغاير. وحقق QR-UKF أدنى متوسط لمربع خطأ تيار المحور q بين المرشحات المتكيفة. كما سجل MSQ-UKF أدنى مئين خامس وتسعين لمتوسط مربع خطأ السرعة بين هذه المرشحات، مع بقاء قيمتي المرشحين الثابت والمرجعي R-oracle أقل منه. وتدعم النتائج اختيار MSQ-UKF عندما تكون الأولوية لمتوسط دقة تقدير السرعة وتتبع التغاير تحت الاضطرابات المختبرة.

الكلمات المفتاحية

المحرك المتزامن ذو المغناطيس الدائم
تقدير الحالة دون مستشعرات
مرشح كالمان التكيفي UKF
تغاير ضوضاء القياس
الاتساق الإحصائي
محاكاة مونت كارلو

Introduction

Permanent magnet synchronous motors (PMSMs) are widely used in high-performance drive systems for their high efficiency, torque density, and dynamic response. Sensorless operation eliminates the need for mechanical speed or position sensors and estimates the required mechanical variables from the motor model and electrical measurements. This reduces hardware requirements and can improve drive reliability. However, state-estimation accuracy can

*Corresponding author
https://doi.org/10.63318/waujpasv4i2_44

deteriorate when motor parameters, operating conditions, or measurement-noise characteristics change [1, 2].

Measurement noise is especially important in sensorless PMSM estimation because the measured electrical signals provide indirect information about the mechanical states. Changes in current-sensor noise can therefore affect estimates of current, rotor speed, and position. A filter that assumes constant noise statistics may become less accurate when sensor conditions change. Online adjustment of the measurement covariance can help the estimator respond to these changes.

The extended Kalman filter (EKF) is widely used for nonlinear PMSM state and parameter estimation [3, 4]. It linearizes the nonlinear model and repeatedly computes the Jacobian matrix. This linearization can reduce estimation accuracy when the operating point changes rapidly or when the observer model differs from the actual motor. The unscented Kalman filter (UKF) avoids explicit linearization by propagating a set of sigma points through the nonlinear model [2, 5]. Consequently, it has been applied to PMSM speed and position estimation, parameter identification, and model-based control [2, 6].

A standard UKF remains sensitive to the selected covariance matrices and sigma-point parameters [5, 7]. In many implementations, the process-noise covariance Q and measurement-noise covariance R are set before operation and then kept fixed [8]. This assumption becomes less suitable when current-sensor noise changes due to temperature, electromagnetic interference, sensor aging, or signal drift. If R is set too low, the filter gives excessive weight to noisy measurements. If it is set too high, it suppresses useful measurement information. Both cases can increase estimation error and degrade statistical consistency [7, 8].

Adaptive covariance methods address this problem by estimating or updating the covariance during operation. The innovation-energy method used in UKF-QR uses an exponentially weighted average of recent innovation energy, following the general approach of innovation-based adaptation [9]. Its adaptation coefficient balances rapid response to noise changes with smooth covariance estimation. The Sage-Husa method used in UKF-SH recursively estimates noise statistics from filter residuals. In practice, its covariance update is bounded to preserve positive definiteness and numerical stability [10]. The master-slave structure used in UKF-MSQ assigns estimation of the measurement-noise variances to a secondary filter, while the main UKF estimates the motor states [11]. This separation can yield smoother estimates of the individual covariance channels, but it also introduces additional parameters and computations.

Sang et al. incorporated a modified Sage–Husa covariance estimator into an adaptive EKF for sensorless PMSM control [10]. They did not compare the three R-adaptive UKF structures examined here. Muñoz et al. developed a master–slave UKF for grid-frequency estimation [11], in which the plant model, estimated states, and disturbances differ from those of a PMSM drive. LaMountain et al. proposed a Bayesian approach to innovation-covariance estimation in sigma-point filters under nonstationary measurement noise [8], but did not evaluate it in a comparative PMSM study. González-Cagigal et al. compared EKF and UKF formulations for sensorless control of a permanent-magnet-assisted synchronous reluctance machine [12]. Their study compared conventional filter formulations rather than alternative online R-adaptation mechanisms.

These studies address related estimation problems, but their results do not show how the covariance-adaptation methods compare on a common PMSM problem. To the best of the authors' knowledge, no published study has directly compared innovation-energy, master-slave, and bounded Sage-Husa R-adaptation using the same PMSM model, initial conditions, voltage inputs, current measurements, operating trajectory, and noise realizations. The available studies also do not compare these methods under both isolated measurement-noise changes and combined parameter and operating disturbances.

Research Gap and Contributions

This study addresses this comparison gap by evaluating three independently tuned adaptive filters: an exponentially weighted innovation-based UKF (UKF-QR), a master–slave UKF (UKF-MSQ), and a bounded Sage-Husa UKF (UKF-SH). A fixed-R UKF serves as a practical baseline for assessing the benefit of covariance adaptation. An oracle-R UKF, which receives the true time-varying measurement covariance at each sampling instant, provides a reference with the exact measurement-noise covariance. All five filters process the same voltage inputs and noisy dq-current measurements along a common nonlinear PMSM trajectory.

The study examines whether the choice of R-adaptation method yields meaningful differences in estimation accuracy, statistical consistency, covariance tracking, and robustness, with all other test conditions held constant. The comparison focuses on the estimators and their covariance-update mechanisms. The five filters operate independently and do not exchange or combine their state estimates.

The main contributions of this paper are as follows:

1. We develop a unified testing framework in which all filter variants use the same initial conditions, voltage inputs, and current measurements. They are evaluated along the same nonlinear PMSM operating trajectory under linear quadratic integral (LQI) speed control. This framework isolates the effect of each covariance-adaptation mechanism and enables a controlled comparison.
2. We apply an independent optimization and evaluation procedure to the adaptive filters. Bayesian optimization first identifies the adaptation parameter for each filter. The parameter is then tested across several development scenarios and refined using a local search. The selected parameters are fixed before the final Monte Carlo evaluation, reducing manual-tuning bias and avoiding adjustments based on the final results.
3. We evaluate the filters using two Monte Carlo studies, each with 50 trials. The first study isolates changes in measurement noise. The second study combines measurement-noise variation with motor-parameter mismatch, speed changes, and load disturbances. The evaluation considers mean squared error (MSE), the standard deviation and 95th percentile of MSE, normalized innovation squared (NIS), reduced-state normalized estimation error squared (NEES), root mean squared error (RMSE) of covariance tracking, and covariance-settling time.

Methodology

Nonlinear PMSM and LQI-Controlled Evaluation

The PMSM is represented in the synchronously rotating dq reference frame by the state vector $\mathbf{x} = \left[i_d,\, i_q,\, \omega,\, \theta\right]^T$, the input vector $\mathbf{u} = [v_d, v_q]^T$, and the measured-current vector $\mathbf{y} = [i_d, i_q]^T$. The model assumes sinusoidal windings and negligible iron losses [13]. The electrical and mechanical dynamics are

$$\dot{i}_d = \frac{v_d - R_s i_d + \omega L_q i_q}{L_d},$$
$$\dot{i}_q = \frac{v_q - R_s i_q - \omega(L_d i_d + \lambda_f)}{L_q}, \quad (1)$$
$$\dot{\omega} = \frac{T_e - T_L - B\omega}{J}, \qquad \dot{\theta} = \omega.$$

where the electromagnetic torque is

$$T_e = \frac{3}{2} p[\lambda_f i_q + (L_d - L_q) i_d i_q]. \quad (2)$$

Here, R_s is stator resistance; L_d and L_q are the d- and q-axis inductances; λ_f is permanent-magnet flux linkage; p is the number of pole pairs; J is rotor inertia; B is the viscous friction coefficient; T_L is load torque; and T_e is electromagnetic torque. The states ω and θ denote the angular speed and integrated angular position used in the implemented model. A fourth-order Runge–Kutta method discretizes the equations at the same sampling interval for the plant and all observers.

$$\mathbf{x}_{k+1} = \mathbf{f}_d(\mathbf{x}_k, \mathbf{u}_k, T_{L,k}) + \mathbf{w}_k, \quad (3)$$

$$\mathbf{y}_k = \mathbf{h}(\mathbf{x}_k) + \mathbf{v}_k, \qquad \mathbf{h}(\mathbf{x}_k) = [i_{d,k} \quad i_{q,k}]^T.$$

where $\mathbf{f}_d(\cdot)$ denotes the RK4 state-transition map, $\mathbf{w}_k \sim \mathcal{N}(\mathbf{0}, \mathbf{Q}_0)$, and $\mathbf{v}_k \sim \mathcal{N}(\mathbf{0}, \mathbf{R}_k)$. The process covariance $\mathbf{Q}_0$ is fixed in all estimators, while $\mathbf{R}_k$ is either fixed, supplied by the oracle reference, or adapted online.

An LQI speed controller generates the reference operating trajectory. LQR-based PMSM speed-control designs use the speed error and its integral [14]. Here, the controller is designed using a discrete linearization at the nominal operating point, with integral action on the speed-tracking error and gains obtained from the discrete Riccati equation. The implemented recursion and control law are

$$z_{k+1} = z_k + T_s(\omega_{\mathrm{ref},k} - \omega_k),$$
$$\mathbf{u}_k = \mathbf{u}_0 - \mathbf{K}_x \,\delta\mathbf{x}_{c,k} - \mathbf{K}_i z_k. \quad (4)$$

Voltage saturation, reference-rate limiting, and anti-windup are applied identically across all trials. The LQI controller uses the true simulated plant state to generate a single trajectory. Each of the five observers receives the resulting dq voltages and noisy dq-current measurements and computes its own state estimate. Figure 1 shows this simulation arrangement. It compares estimator behavior with supplied dq signals; closed-loop sensorless control and coordinate generation remain outside the present evaluation.

Unscented Kalman Filter and Reference Estimators

For the state and measurement dimensions $n = 4$ and $m = 2$, respectively, the scaled UKF uses $\lambda = \alpha^2(n + \kappa) - n$. The parameters α, β, κ control the sigma-point spread and weighting; $\beta = 2$ is used for the Gaussian prior. The sigma points and their standard mean and covariance weights are defined as in [5].

$$\boldsymbol{\chi}^{(0)}_{k-1|k-1} = \hat{\mathbf{x}}_{k-1|k-1},$$
$$\boldsymbol{\chi}^{(i)}_{k-1|k-1} = \hat{\mathbf{x}}_{k-1|k-1} + \left[\sqrt{(n+\lambda)\mathbf{P}_{k-1|k-1}}\right]_i,$$
$$\boldsymbol{\chi}^{(i+n)}_{k-1|k-1} = \hat{\mathbf{x}}_{k-1|k-1} - \left[\sqrt{(n+\lambda)\mathbf{P}_{k-1|k-1}}\right]_i,$$

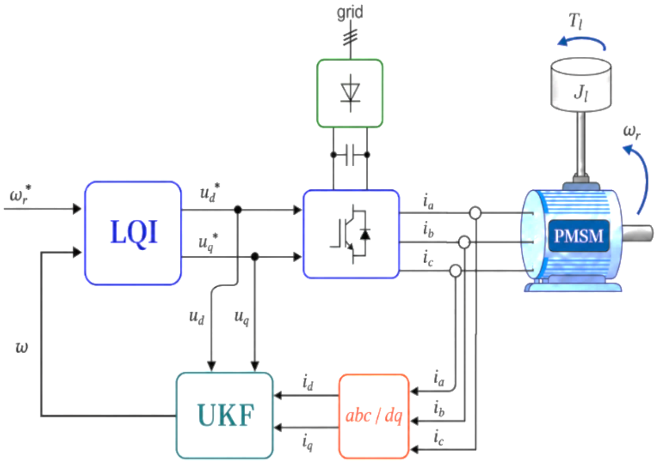

Figure 1: Common-trajectory simulation and independent evaluation of the five observers. Only the oracle-R observer receives the true measurement covariance

$$i = 1, \ldots, n,$$
$$W_0^{(m)} = \frac{\lambda}{n+\lambda}, \qquad W_0^{(c)} = \frac{\lambda}{n+\lambda} + 1 - \alpha^2 + \beta, \quad (5)$$
$$W_i^{(m)} = W_i^{(c)} = \frac{1}{2(n+\lambda)}, \qquad i = 1, \ldots, 2n.$$

Each sigma point is propagated through the RK4-discretized PMSM model. The predicted state and covariance are

$$\chi^{(i)}_{k|k-1} = f_d\left(\chi^{(i)}_{k-1|k-1}, u_{k-1}, T_{L,k-1}\right),$$
$$\hat{x}_k^- = \sum_{i=0}^{2n} W_i^{(m)} \chi^{(i)}_{k|k-1}.$$
$$\Delta\chi_{i,k} = \chi^{(i)}_{k|k-1} - \hat{x}_k^-, \quad (6)$$
$$P_k^- = \sum_{i=0}^{2n} W_i^{(c)} \Delta\chi_{i,k} \Delta\chi_{i,k}^T + Q_0.$$

The propagated sigma points are then mapped through the current-measurement function. The predicted measurement, predicted measurement dispersion $\boldsymbol{\Omega}_{y,k}$, innovation covariance, and state–measurement cross-covariance are

$$\boldsymbol{\gamma}_k^{(i)} = \mathbf{h}(\boldsymbol{\chi}^{(i)}_{k|k-1}), \qquad \hat{\mathbf{y}}_k^- = \sum_{i=0}^{2n} W_i^{(m)} \boldsymbol{\gamma}_k^{(i)}.$$
$$\Delta\boldsymbol{\gamma}_{i,k} = \boldsymbol{\gamma}_k^{(i)} - \hat{\mathbf{y}}_k^-, \qquad \boldsymbol{\Omega}_{y,k} = \sum_{i=0}^{2n} W_i^{(c)} \Delta\boldsymbol{\gamma}_{i,k} \Delta\boldsymbol{\gamma}_{i,k}^T. \quad (7)$$
$$\mathbf{S}_k = \boldsymbol{\Omega}_{y,k} + \mathbf{R}_k, \qquad \mathbf{P}_{xy,k} = \sum_{i=0}^{2n} W_i^{(c)} \Delta\boldsymbol{\chi}_{i,k} \Delta\boldsymbol{\gamma}_{i,k}^T.$$

The innovation, Kalman gain, corrected state estimate, and corrected covariance are

$$\mathbf{v}_k = \mathbf{y}_k - \hat{\mathbf{y}}_k^-, \qquad \mathbf{K}_k = \mathbf{P}_{xy,k}\mathbf{S}_k^{-1}.$$
$$\hat{\mathbf{x}}_k = \hat{\mathbf{x}}_k^- + \mathbf{K}_k \mathbf{v}_k, \qquad \mathbf{P}_k = \mathbf{P}_k^- - \mathbf{K}_k \mathbf{S}_k \mathbf{K}_k^T. \quad (8)$$
$$\mathbf{P}_k \leftarrow \frac{1}{2}(\mathbf{P}_k + \mathbf{P}_k^T).$$

The covariance is symmetrized after each correction, and a small diagonal regularization term is added only if the Cholesky factorization fails. The fixed UKF uses $\mathbf{Q}_k = \mathbf{Q}_0$ and $\mathbf{R}_k = \mathbf{R}_0$ throughout the simulation. The oracle-R UKF uses the same recursion and fixed $\mathbf{Q}_0$ but receives the exact scheduled covariance $\mathrm{R}(t)$ at each sample. It is included only as an ideal reference for the measurement covariance.

Algorithm 1. Common UKF State Estimation

Inputs: $\hat{\mathbf{x}}_{k-1}^{+}$, $\mathbf{P}_{k-1}^{+}$, $\mathbf{u}_{k-1}$, $\mathbf{y}_k$, $\mathbf{Q}_0$, and $\mathbf{R}_k$.

1. Generate the sigma points and weights using Equation (5).
2. Propagate the sigma points through the discrete PMSM model.
3. Calculate the predicted state and covariance using Equation (6).
4. Map the propagated sigma points through the measurement model and calculate $\hat{\mathbf{y}}_k^{-}$, $\mathbf{\Omega}_{\gamma,k}$, $\mathbf{S}_k$, and $\mathbf{P}_{x\gamma,k}$ using Equation (7).
5. Calculate the innovation and Kalman gain, and correct the state and covariance using Equation (8).
6. Symmetrize $\mathbf{P}_k^{+}$ and add a small diagonal regularization term only when required.
7. For an adaptive observer, use the innovation at sample k to calculate R_{k+1} after the state correction. The correction at sample k uses the previously available R_k. The fixed observer retains R_0, and the oracle uses the scheduled covariance.

Outputs: $\hat{x}_k^{+}$, P_k^{+}, ν_k, and, for an adaptive observer, R_{k+1}.

All five observers use the same UKF prediction and correction equations. They differ in how they supply or update the measurement covariance. The slave filter belongs only to UKF-MSQ and estimates the two diagonal covariance entries. No state estimates are exchanged between observers.

R-Adaptive UKF Structures

The UKF-QR variant uses an exponentially weighted innovation-energy recursion motivated by innovation-based adaptation [9]. Only the two measured-current variances are updated, and $\mathbf{Q}_k = \mathbf{Q}_0$ remains unchanged. The implemented diagonal update is

$$\mathbf{R}_{k+1} = \Pi_R\left[(1-\alpha_R)\mathbf{R}_k + \alpha_R \mathrm{diag}\left(\nu_{1,k}^2, \nu_{2,k}^2\right)\right]. \quad (9)$$

where $\boldsymbol{\nu}_k$ is the current innovation and α_R controls the adaptation rate.

This update averages innovation energy without subtracting the predicted measurement dispersion. It therefore provides an effective measurement covariance and need not recover the physical sensor-noise variance exactly.

The UKF-MSQ uses a main UKF for state estimation and a low-dimensional slave filter for the two measurement-noise variances [11]. The variance vector and innovation-based pseudo-measurement are

$$\mathbf{r}_k = [R_{11,k} \quad R_{22,k}]^T, \\ \mathbf{z}_k^R = \left[\nu_{1,k}^2 - \Omega_{y,11,k} \quad \nu_{2,k}^2 - \Omega_{y,22,k}\right]^T. \quad (10)$$

The slave-filter's prediction, correction, covariance update, and smoothed variance, provided to the master UKF, are

$$\begin{gathered}\hat{\mathbf{r}}_k^{-} = \hat{\mathbf{r}}_{k-1}, \qquad \mathbf{P}_k^{R,-} = \mathbf{P}_{k-1}^{R} + \mathbf{Q}_R. \\ \mathbf{K}_k^R = \mathbf{P}_k^{R,-}\left(\mathbf{P}_k^{R,-} + \mathbf{R}_R\right)^{-1}. \\ \hat{\mathbf{r}}_k = \hat{\mathbf{r}}_k^{-} + \mathbf{K}_k^R(\mathbf{z}_k^R - \hat{\mathbf{r}}_k^{-}). \\ \mathbf{P}_k^R = (\mathbf{I}-\mathbf{K}_k^R)\mathbf{P}_k^{R,-}(\mathbf{I}-\mathbf{K}_k^R)^T + \mathbf{K}_k^R\mathbf{R}_R(\mathbf{K}_k^R)^T. \\ \bar{\mathbf{r}}_k = (1-\beta_{\mathrm{MS}})\bar{\mathbf{r}}_{k-1} + \beta_{\mathrm{MS}}\hat{\mathbf{r}}_k, \qquad \mathbf{R}_{k+1} \\ = \Pi_R[\mathrm{diag}(\bar{\mathbf{r}}_k)].\end{gathered} \quad (11)$$

where $\hat{\mathbf{r}}_k$ is the internal slave estimate, and $\bar{\mathbf{r}}_k$ is the smoothed output used by the master filter. This distinction keeps the slave's covariance update consistent with its Kalman gain while allowing β_{MS} to control output smoothing.

The UKF-SH applies a bounded Sage–Husa-type update to the measurement covariance [10]. The recursion subtracts the predicted measurement dispersion in Equation (7) from the innovation energy before updating each covariance channel:

$$d_k = \left[\nu_{1,k}^2 - \Omega_{y,11,k},\ \nu_{2,k}^2 - \Omega_{y,22,k}\right]^T, \\ R_{k+1} = \Pi_R[(1-\gamma_R)R_k + \gamma_R \mathrm{diag}(d_k)]. \quad (12)$$

The channel-wise form in (12) preserves the assumed diagonal measurement-covariance structure, while the scalar adaptation coefficient controls the update rate.

All adaptive methods use the same lower and upper covariance limits. For a symmetric candidate matrix, the positive-definite projection is

$$\mathbf{M}_s = 1/2\,(\mathbf{M}+\mathbf{M}^T) = \mathbf{U}\mathrm{diag}(\lambda_i)\mathbf{U}^T, \\ \Pi_R(\mathbf{M}) = \mathbf{U}\mathrm{diag}(\min\{\max(\lambda_i, \lambda_{\min}), \lambda_{\max}\})\mathbf{U}^T. \quad (13)$$

where $\lambda_{\min} > 0$. The projection preserves symmetry and positive definiteness and prevents isolated innovation samples from producing nonphysical variances.

Independent Parameter Tuning

We tune each scalar adaptation coefficient independently using Bayesian optimization [15]. The search uses a common development set, followed by confirmation over twenty scenarios and local refinement. The objective combines normalized post-change MSE for i_d, i_q, and ω. Candidate settings must also avoid numerical failure, maintain acceptable NIS, and rarely reach the covariance bounds. Near-optimal candidates are compared using innovation consistency, covariance-tracking RMSE, and settling time. The selected coefficients are fixed before testing on independent Monte Carlo seeds. Data-based tuning has also been applied to electrohydraulic PID control using radial-basis-function

Metamodeling [16-18]; the present procedure instead selects estimator adaptation coefficients.

The final coefficients were

$$\alpha_R = 1.6541\times10^{-4}, \qquad \beta_{MS} = 3.3013\times10^{-2}, \\ \gamma_R = 1.9673\times10^{-4}.$$

The MSQ slave parameters were

$$\mathbf{P}_0^R = 10^{-2}\mathbf{I}, \quad \mathbf{Q}_R = 10^{-7}\mathbf{I}, \quad \mathbf{R}_R = 10^{-3}\mathbf{I}.$$

Performance Measures

The comparison combines state-estimation accuracy, covariance tracking, and statistical consistency. For the state component i_d, i_q, or ω, the Monte Carlo MSE is

$$\mathrm{MSE}_j = \frac{1}{N_{\mathrm{MC}}}\sum_{r=1}^{N_{\mathrm{MC}}}\frac{1}{N}\sum_{k=1}^{N}\left(x_{j,k}^{(r)} - \hat{x}_{j,k}^{(r)}\right)^2. \quad (14)$$

Innovation consistency is quantified by the normalized innovation squared:

$$\mathrm{NIS}_k = \boldsymbol{\nu}_k^T\mathbf{S}_k^{-1}\boldsymbol{\nu}_k. \quad (15)$$

Because the adopted dq model obtains rotor position by integrating speed, we evaluate state-covariance consistency for the reduced state containing i_d, i_q, and ω:

The supplied dq-current measurements do not directly correct an initial position offset in this model. The quantitative state comparison therefore concerns the two currents and rotor speed.

$$\mathrm{NEES}_{3,k} = \tilde{\mathbf{x}}_{3,k}^T\mathbf{P}_{3,k}^{-1}\tilde{\mathbf{x}}_{3,k}, \\ \tilde{\mathbf{x}}_{3,k} = [i_{d,k} - \hat{\imath}_{d,k} \quad i_{q,k} - \hat{\imath}_{q,k} \quad \omega_k - \widehat{\omega}_k]^T. \quad (16)$$

For a consistent filter with a two-dimensional measurement vector, the reference mean NIS is 2; the corresponding mean NEES_3 is 3. These values are used as descriptive consistency checks. We also report covariance-tracking RMSE, settling time after each covariance transition, and the standard deviation and 95th percentile of trial-wise MSE. Settled-window calculations exclude the first 1 s after each covariance transition and, in the combined-stress case, the operating-transition interval.

Simulation Setup

All observers are evaluated in MATLAB using the same RK4-discretized PMSM model. Each trial lasts 20 s. The noise-only case uses matched plant and observer parameters, a constant 300 rad/s speed reference, and zero external load torque. The combined-stress case uses the same noise schedule, with L_d, L_q, R_s, and J independently sampled from uniform distributions spanning 80–120% of their nominal values.

In the combined-stress case, speed-reference changes begin at t = 2, 6, 10, 14, and 18 s. The six reference levels are 300, 180, 260, 140, 230, and 200 rad/s, with a rate limit of 2000 rad/s². The load profile takes the successive values 0, 0.25, 0.10, −0.20, 0.05, 0.30, −0.10, −0.30, 0.15, 0.25, and 0 N·m during the test.

The sampling interval is 1×10^{-4} s. The nominal parameters are L_d =1.5 mH, L_q =2 mH, R_s =0.01 Ω, J=0.01 kg·m², B=0.001 N·m·s, λ_f =0.1 Wb, and four pole pairs. The nominal operating point is i_d=0 A, i_q =0.5 A, and ω=300 rad/s, and the voltage magnitude is limited to 50 V. All observers use α = 0.1, β = 2, and κ = 0, with

$$P_0 = \mathrm{diag}(0.05^2, 0.05^2, 5^2, 0.05^2),$$

$$Q_0 = \mathrm{diag}(3 \times 10^{-5}, 3 \times 10^{-5}, 10^{-4}, 10^{-6}) .$$

Adaptation begins after 0.5 s. The true current-measurement covariance follows five consecutive 4 s regimes. The initial interval represents the correctly initialized low-noise condition. It is followed by asymmetric increases in variance, a simultaneous high-noise condition, and a final recovery stage defined by:

$$R(t) = \mathrm{diag}\big(r_{11}(t), r_{22}(t)\big),$$

$$\big(r_{11}(t), r_{22}(t)\big) = \begin{cases} (0.00125,\ 0.005), & 0 \le t < 4\,\mathrm{s}, \\ (0.08,\ 0.015), & 4 \le t < 8\,\mathrm{s}, \\ (0.012,\ 0.12), & 8 \le t < 12\,\mathrm{s}, \\ (0.07,\ 0.09), & 12 \le t < 16\,\mathrm{s}, \\ (0.008,\ 0.012), & 16 \le t \le 20\,\mathrm{s}. \end{cases}$$

The fixed UKF retains the initial covariance R_0 throughout the simulation. The oracle-R UKF receives the exact scheduled R(t), while the adaptive observers update R online. Each 4 s regime is divided into four 1 s analysis intervals: the covariance transition, post-transition settling, an operating transition, and final settled operation. In the noise-only test, the operating point remains constant, so the third interval supplies an additional settled period.

Each scenario is repeated for 50 Monte Carlo trials. Within a trial, all observers receive the same plant trajectory and noise realization. No explicit process-noise sequence is added to the plant; Q_0 is a fixed observer design covariance. Results are calculated over the full post-change intervals and the predefined settled high-noise windows.

Simulation Procedure

1) Select a Monte Carlo seed and, for the combined-stress case, sample the plant parameters.

2) Simulate the plant with true-state LQI feedback, the voltage limit, reference-rate limit, and anti-windup. Record the common dq-voltage inputs and noisy current measurements.

3) Run the fixed-R, oracle-R, UKF-QR, UKF-MSQ, and UKF-SH observers independently on the same record.

4) At each sample, predict and correct the state using R_k. For an adaptive observer, then calculate R_{k+1} from the current innovation.

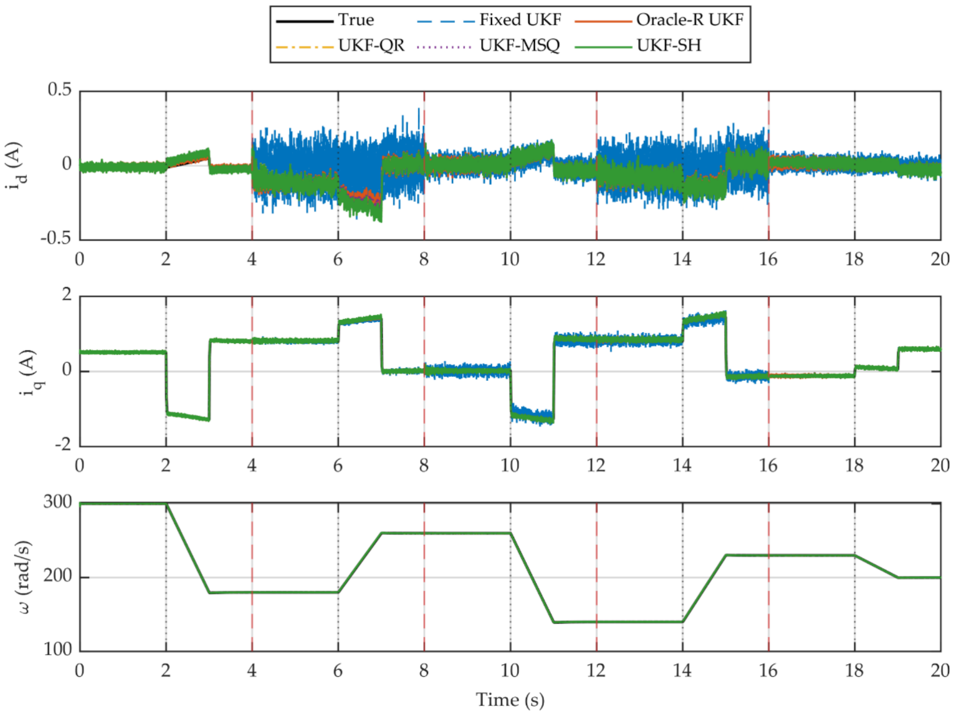

Figure 2: Representative i_d, i_q, and rotor-speed trajectories in the combined-stress experiment. Black dotted lines indicate operating transitions, and red dashed lines indicate measurement-covariance transitions

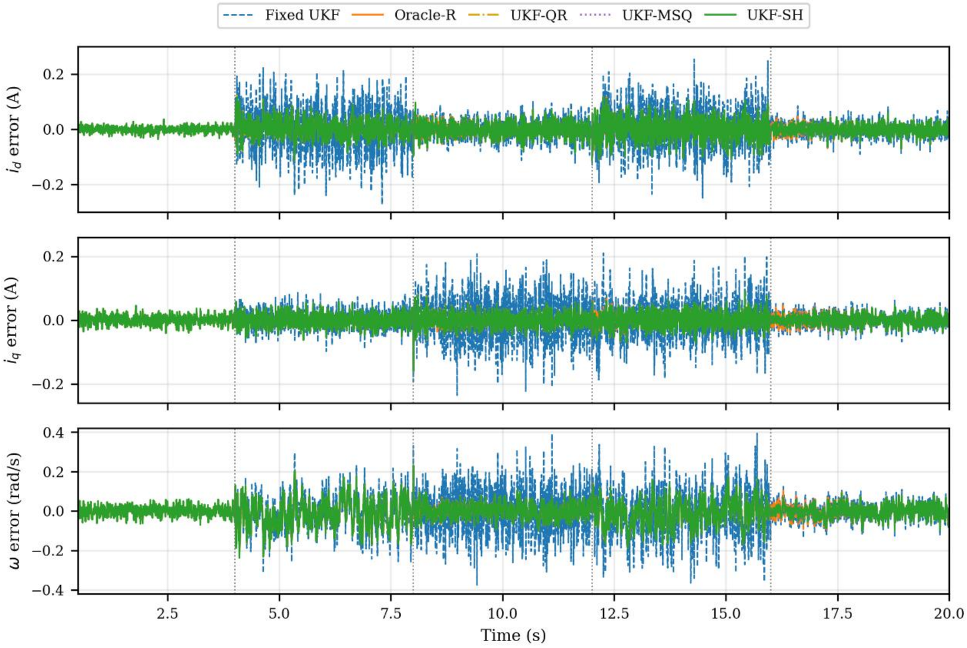

Figure 3: Representative state-estimation errors in the noise-only repeated-covariance test.

5) Repeat for 50 seeds per scenario, using the same realization for all observers in each trial.

6) Calculate the accuracy, consistency, covariance-tracking, settling-time, and trial-wise statistics over the specified windows, with no further tuning.

Results and Discussion

Time-Domain Behavior

Figure 2 shows the current and speed estimates during the combined-stress test. The estimated speed follows the six reference levels, and the observer traces largely overlap. The clearest differences appear in i_d during high-noise intervals. The fixed UKF retains the low initial R_0 and gives excessive weight to the noisy measurements, producing larger current fluctuations. The black dotted lines mark operating changes, which introduce short transients; the red dashed lines mark changes in measurement covariance, which mainly affect the error fluctuation level. Each trace is the output of a separate observer.

Figure 3 shows the noise-only test, in which the plant and observer parameters match. Current-error fluctuations increase as measurement noise rises and then decrease in the final, lower-noise regime after t = 16 s. The fixed UKF exhibits the largest fluctuations because it retains the initial low R_0. Once their covariance estimates converge, the adaptive observers reduce the influence of noisy measurements, consistent with the lower MSE values in Table 1.

Settled-State Estimation Accuracy

Table 1 reports the MSE over the predefined settled high-noise windows, excluding the first second after each covariance transition. Relative to the fixed UKF, the adaptive filters reduce the i_d, i_q, and speed MSE by about 80%, 86%, and 70-71%, respectively. UKF-QR yields the lowest mean MSE across all three states and closely approaches the oracle-R reference. However, the largest difference among the adaptive means is only 3.4%. This small difference indicates that the adaptive filters perform similarly in the noise-only test.

Under combined stress, the innovation contains both measurement noise and model error. Table 2 and Figure 4 show that UKF-MSQ gives the lowest i_d and speed MSE among the adaptive observers, whereas UKF-QR gives the lowest i_q MSE. The i_q differences are small. The oracle-R UKF has the lowest mean MSE for all three states in this test, but its elevated $NEES_3$ shows that exact measurement covariance does not by itself resolve the uncertainty caused by model mismatch.

Innovation and State-Covariance Consistency

Tables 1 and 2 report the mean NIS and reduced-state NEES3 values, and Figure 5 compares them with the theoretical means. The fixed UKF yields NIS values near 43 in both scenarios, indicating severe inconsistency when the measurement covariance changes. In contrast, the oracle-R UKF and the adaptive filters maintain mean NIS values near the theoretical value of two. These mean values suggest that adapting R improves the balance between predicted measurement uncertainty and the observed innovations. However, they do not, on their own, establish full statistical consistency.

In the noise-only case, the oracle and adaptive observers yield mean $NEES_3$ values below 3, indicating that the state-covariance estimates are conservative on average. Under combined stress, their mean $NEES_3$ values exceed 3. This is consistent with parameter-induced model errors that the fixed Q_0 does not adequately capture. Adapting R improves measurement weighting, but it cannot eliminate errors in the motor dynamics.

Measurement-Covariance Tracking

Figure 6 and Table 3 compare the covariance-tracking performance of the adaptive filters. UKF-MSQ yields the lowest average RMSE for both R_{11} and R_{22} and the shortest mean settling times across both test scenarios. UKF-QR, however, achieves the lowest settled-window state-estimation MSE in the noise-only test, whereas UKF-SH generally provides intermediate tracking performance. These findings indicate that more accurate covariance tracking does not necessarily reduce state-estimation error.

The transition-specific results also show that the filter response depends on whether the covariance increases or decreases. UKF-MSQ responds fastest to several downward

Table 1: Noise-only settled-window MSE and whole post-change NIS/NEES₃. MSE reductions relative to the fixed UKF are shown in parentheses.

Method	i_d MSE (A^2)	i_q MSE (A^2)	ω MSE $(rad/s)^2$	Mean NIS	Mean $NEES_3$
Fixed UKF	4.522×10^{-3}	3.056×10^{-3}	1.136×10^{-2}	42.711	25.424
Oracle-R UKF	8.761×10^{-4} (80.6%)	4.176×10^{-4} (86.3%)	3.275×10^{-3} (71.2%)	1.964	1.130
UKF-QR	8.722×10^{-4} (80.7%)	4.173×10^{-4} (86.3%)	3.282×10^{-3} (71.1%)	2.024	1.178
UKF-MSQ	9.014×10^{-4} (80.1%)	4.315×10^{-4} (85.9%)	3.355×10^{-3} (70.5%)	2.105	1.213
UKF-SH	8.813×10^{-4} (80.5%)	4.227×10^{-4} (86.2%)	3.303×10^{-3} (70.9%)	2.083	1.211

Table 2: Combined-stress settled-window MSE and whole post-change NIS/NEES₃; reductions relative to the fixed UKF are shown in parentheses.

Method	i_d MSE (A^2)	i_q MSE (A^2)	ω MSE $(rad/s)^2$	Mean NIS	Mean $NEES_3$
Fixed UKF	4.417×10^{-3}	3.257×10^{-3}	9.970×10^{-3}	42.914	26.533
Oracle-R UKF	2.677×10^{-3} (39.4%)	1.129×10^{-3} (65.3%)	6.571×10^{-3} (34.1%)	2.054	5.864
UKF-QR	3.154×10^{-3} (28.6%)	1.134×10^{-3} (65.2%)	8.630×10^{-3} (13.4%)	2.019	6.254
UKF-MSQ	2.809×10^{-3} (36.4%)	1.145×10^{-3} (64.8%)	7.265×10^{-3} (27.1%)	2.116	6.101
UKF-SH	3.196×10^{-3} (27.6%)	1.142×10^{-3} (65.0%)	8.777×10^{-3} (12.0%)	2.078	6.340

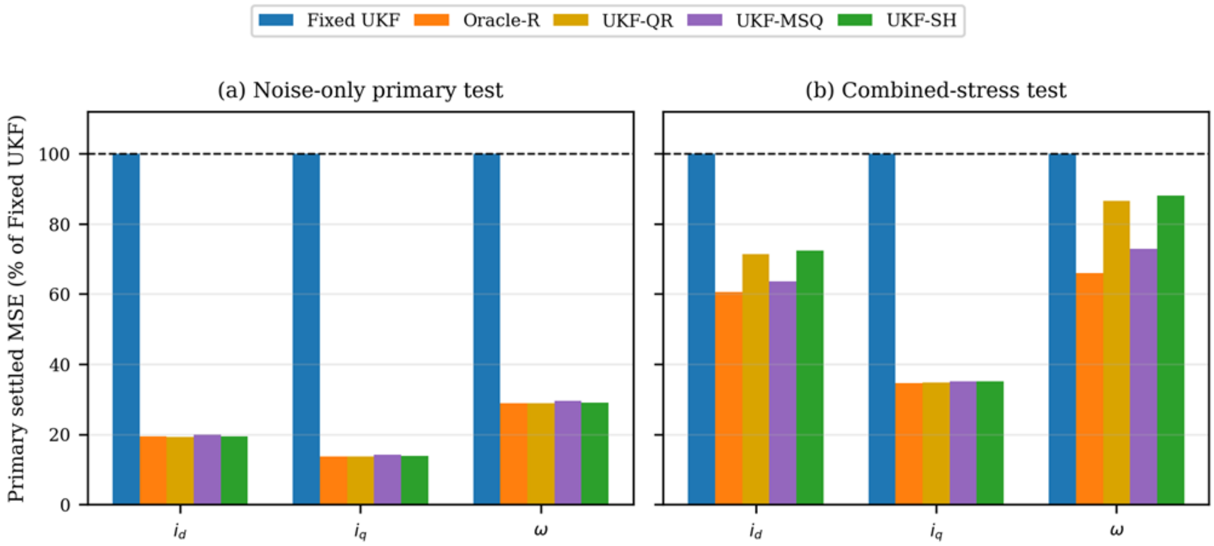

Figure 4: Primary settled-window MSE in the noise-only and combined-stress tests, normalized to the corresponding fixed-UKF result.

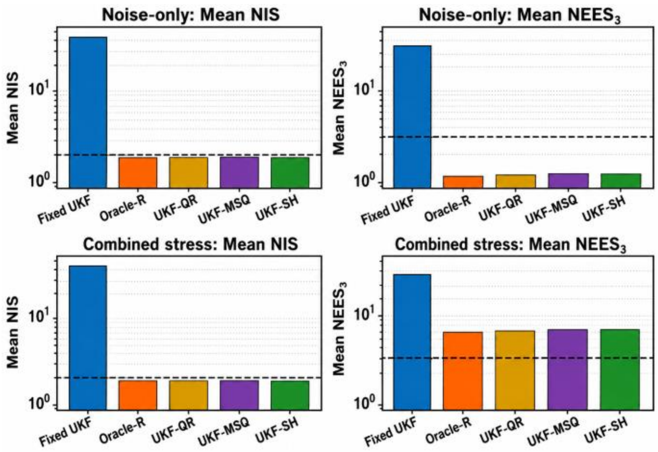

Figure 5: Mean NIS and reduced-state NEES₃ in the two tests. Dashed lines denote the theoretical means

transitions, whereas UKF-SH gives the shortest settling time for the large increase in R_{22} from 0.015 to 0.120. A similar response is observed in the combined-stress scenario.

In the combined-stress test, the R_{11} estimate overshoots when operating-point and load changes occur near a covariance transition. In this scenario, the innovation reflects the combined effects of measurement noise and model mismatch. The adapted covariance should therefore be interpreted as an effective covariance that maintains innovation consistency rather than as a direct estimate of the physical sensor-noise variance.

Table 3: Mean post-change covariance-tracking RMSE (A^2), with mean settling time (s) in parentheses, across repeated covariance transitions.

Method	Noise-only R_{11}	Noise-only R_{22}	Combined stress R_{11}	Combined stress R_{22}	Observed strength
UKF-QR	0.01842 (1.370)	0.01849 (1.391)	0.02390 (1.450)	0.01877 (1.380)	Lowest isolated MSE
UKF-MSQ	0.01365 (1.013)	0.01440 (0.846)	0.01560 (0.946)	0.01423 (0.812)	Best average *R* tracking
UKF-SH	0.01673 (1.163)	0.01691 (1.196)	0.02271 (1.212)	0.01708 (1.178)	Fastest selected increases

Monte Carlo Robustness

Table 4 reports the standard deviation and 95th percentile of MSE across the 50 trials. Variation is small in the noise-only test and increases under combined stress, particularly for i_d and speed. Among the adaptive observers, UKF-MSQ gives the lowest 95th-percentile speed MSE, 1.689×10^{-2} $(rad/s)^2$, compared with 2.234×10^{-2} for UKF-QR and 2.324×10^{-2} for UKF-SH. The fixed and oracle-R observers give lower speed percentiles, 1.052×10^{-2} and 1.376×10^{-2} $(rad/s)^2$, respectively. UKF-MSQ therefore improves the upper-tail result relative to the other adaptive methods, but not relative to either reference. All observers complete the trials without reported numerical failure or covariance-bound activation.

As shown in Table 2 and Figure 4, the mean MSE under combined stress follows a similar pattern. Among the adaptive filters, UKF-MSQ yields the lowest i_d and speed MSE, whereas UKF-QR yields the lowest i_q MSE. However, UKF-QR's i_q advantage is small.

Table 4: Standard deviation / 95th percentile of trial-wise settled-window MSE over 50 Monte Carlo trials. Current MSE is in A²; speed MSE is in (rad/s)².

Scenario	Method	i_d MSE (A²)	i_q MSE (A²)	ω MSE (rad/s)²
Noise only	Fixed	7.489e-5 / 4.631e-3	5.428e-5 / 3.147e-3	3.055e-4 / 1.187e-2
Noise only	Oracle-R	2.636e-5 / 9.187e-4	1.158e-5 / 4.327e-4	2.036e-4 / 3.588e-3
Noise only	UKF-QR	2.632e-5 / 9.144e-4	1.120e-5 / 4.320e-4	2.035e-4 / 3.598e-3
Noise only	UKF-MSQ	2.684e-5 / 9.445e-4	1.163e-5 / 4.475e-4	2.054e-4 / 3.671e-3
Noise only	UKF-SH	2.638e-5 / 9.234e-4	1.134e-5 / 4.377e-4	2.039e-4 / 3.619e-3
Combined	Fixed	1.042e-4 / 4.568e-3	8.357e-5 / 3.380e-3	3.627e-4 / 1.052e-2
Combined	Oracle-R	1.819e-3 / 5.720e-3	5.553e-4 / 2.035e-3	4.174e-3 / 1.376e-2
Combined	UKF-QR	2.452e-3 / 7.494e-3	5.687e-4 / 2.077e-3	6.993e-3 / 2.234e-2
Combined	UKF-MSQ	1.998e-3 / 6.210e-3	5.558e-4 / 2.063e-3	5.120e-3 / 1.689e-2
Combined	UKF-SH	2.503e-3 / 7.638e-3	5.699e-4 / 2.088e-3	7.232e-3 / 2.324e-2

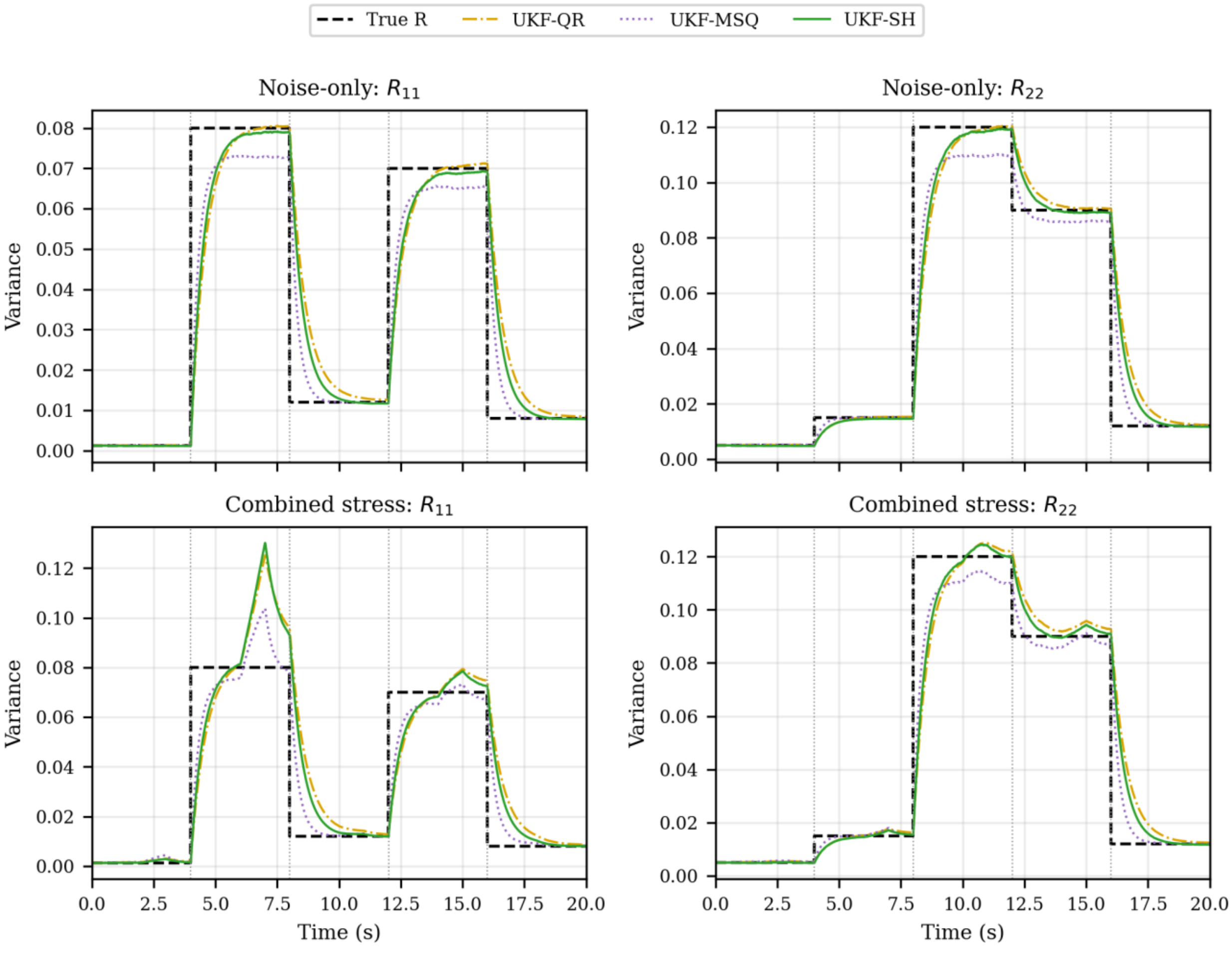

Figure 6: Monte Carlo mean R_{11} and R_{22} estimates during repeated covariance changes in the noise-only and combined-stress tests

Overall Discussion

In the noise-only test, matched dynamics limit the contribution of model error to the innovation, helping explain the low MSE achieved by UKF-QR. Under combined stress, UKF-MSQ smooths fluctuations through its separate variance estimator. This may explain its lower speed MSE and 95th percentile relative to the other adaptive methods. UKF-SH subtracts the predicted measurement dispersion, so errors in that prediction can affect its response. These differences are consistent with the model-error contamination of innovation-based covariance estimates reported by Jiang et al. [19]. Their measurement approach reduces this coupling, suggesting a useful direction for future PMSM comparisons.

Covariance-tracking accuracy and state MSE need not rank the filters in the same order. The Kalman correction also depends on the predicted state covariance and the state–measurement cross-covariance. UKF-MSQ tracks R most accurately on average, yet UKF-QR yields lower state MSE in the noise-only test. Under combined stress, oracle-R yields the lowest mean state MSE. The fixed UKF has a lower 95th-percentile speed MSE than the adaptive methods, despite its poorer mean accuracy and innovation consistency. Filter selection must therefore distinguish average performance from upper-tail performance.

Mean NIS values near two suggest improved innovation consistency. However, the elevated $NEES_3$ under combined stress indicates that the state covariance understates the observed errors. The fixed Q_0 does not explicitly capture the randomized motor-parameter errors, and adjusting R cannot correct biased dynamics. Joint Q–R adaptation or parameter estimation is a useful next step.

Conclusion

This study compared three independently tuned R-adaptive UKFs under identical PMSM test conditions, using fixed-R and oracle-R filters as references. Two 50-trial Monte Carlo tests examined noise-only changes and combined parameter and operating disturbances.

All three adaptive observers reduce mean settled-window MSE and improve mean innovation consistency relative to the fixed UKF. UKF-QR yields the lowest adaptive MSE in the noise-only test. Under combined stress, UKF-MSQ yields the lowest adaptive i_d and speed MSE and provides the best average covariance tracking. It is therefore the strongest of the three adaptive options when average speed accuracy is the primary requirement. However, its upper-tail speed MSE remains higher than that of the fixed and oracle-R references. No method leads across all metrics.

These findings apply to the simulated estimator comparison using common dq measurements. Further work should examine joint Q–R or parameter adaptation, estimator-based closed-loop control, coordinate generation, inverter nonidealities, and hardware validation.

Author Contributions: **Salah**: Conceptualization, methodology, and writing of the original draft. **Abubaker:** Review and editing. All authors read and approved the final manuscript.

Conflicts of Interest: The authors declare no conflict of interest.

Funding: This research received no external funding.

Data Availability Statement: The MATLAB code and simulation data supporting the findings of this study are available from the corresponding author upon reasonable request.

References

[1] G. Wang, M. Valla, and J. Solsona. “Position Sensorless Permanent Magnet Synchronous Machine Drives: A Review.” *IEEE Transactions on Industrial Electronics*, vol. 67, no. 7, pp. 5830–5842, 2020. https://doi.org/10.1109/TIE.2019.2955409

[2] D. Janiszewski. “Sensorless Model Predictive Control of Permanent Magnet Synchronous Motors Using an Unscented Kalman Filter.” *Energies*, vol. 17, no. 10, p. 2387, 2024. https://doi.org/10.3390/en17102387

[3] P. Tety, et al. “A Robust Extended Kalman Filter for Speed-Sensorless Control of a Linearized and Decoupled PMSM Drive.” *Engineering*, vol. 7, no. 10, pp. 691–699, 2015. https://doi.org/10.4236/eng.2015.710060

[4] A. Sel, B. Sel, U. Coskun, and C. Kasnakoglu. “Comparative Study of an EKF-Based Parameter Estimation and a Nonlinear Optimization-Based Estimation on PMSM System Identification.” *Energies*, vol. 14, no. 19, Art. no. 6108, 2021. https://doi.org/10.3390/en14196108

[5] S. Julier, and J. Uhlmann. “Unscented Filtering and Nonlinear Estimation.” *Proceedings of the IEEE*, vol. 92, no. 3, pp. 401–422, 2004. https://doi.org/10.1109/JPROC.2003.823141

[6] D. Janiszewski. “Sensorless PMSM Speed Control Using an FPGA-Implemented Unscented Kalman Filter.” *Applied Sciences*, vol. 16, no. 11, Art. no. 5429, 2026. https://doi.org/10.3390/app16115429

[7] S. Rigon, B. Haus, P. Mercorelli, and M. Zigliotto. “Comparison Between UKF and EKF in Sensorless Synchronous Reluctance Motor Drives,” *IEEE Open Journal of Power Electronics*, vol. 5, pp. 1562–1572, 2024. https://doi.org/10.1109/OJPEL.2024.3469533

[8] G. LaMountain, J. Valls, and P. Closas. “Measurement Noise Covariance Estimation in Gaussian Filters: An Online Bayesian Solution/” *EURASIP Journal on Advances in Signal Processing*, vol. 2025, Art. no. 14, 2025. https://doi.org/10.1186/s13634-025-01215-w

[9] F. Sun, X. Hu, Y. Zou, and S. Li. “Adaptive Unscented Kalman Filtering for State of Charge Estimation of a Lithium-Ion Battery for Electric Vehicles.” *Energy*, vol. 36, no. 5, pp. 3531–3540, 2011. https://doi.org/10.1016/j.energy.2011.03.059

[10] Y. Sang, Z. Wu, and Y. Fan. “An Adaptive Extended Kalman Filter Observer-for Permanent Magnet Synchronous Motor Position Sensorless Control Systems.” *Scientific Reports*, vol. 15, Art. no. 11605, 2025. https://doi.org/10.1038/s41598-025-85787-5

[11] J. Muñoz, M. E. Magaña, and E. Cotilla-Sanchez, “Adaptive Master–Slave Unscented Kalman Filter for Grid Voltage Frequency Estimation.” *IET Signal Processing*, vol. 12, no. 4, pp. 496–505, 2018. https://doi.org/10.1049/iet-spr.2016.0199

[12] M. Cagigal, C. Martín, M. Bermúdez, and P. Romero. “Comparison of Nonlinear Kalman Filtering Schemes for Sensorless Control of Permanent Magnet-Assisted Synchronous Reluctance Machines.” *International Journal of Electrical Power and Energy Systems*, vol. 165, Art. no. 110487, 2025. https://doi.org/10.1016/j.ijepes.2025.110487

[13] P. Pillay and R. Krishnan. “Modeling, Simulation, and Analysis of Permanent-Magnet Motor Drives. I. The Permanent-Magnet Synchronous Motor Drive.” *IEEE Transactions on Industry Applications*, vol. 25, no. 2, pp. 265–273, 1989. https://doi.org/10.1109/28.25541

[14] B. Zhang and W. Zhang. “Speed Loop Control of Permanent Magnet Synchronous Motor Based on Linear Quadratic Regulator Parameter Tuning.” *Optimal Control Applications and Methods*, vol. 46, no. 5, pp. 2153–2164, 2025. https://doi.org/10.1002/oca.3314

[15] B. Shahriari, et al. “Taking the Human Out of the Loop: A Review of Bayesian Optimization.” *Proceedings of the IEEE*, vol. 104, no. 1, pp. 148–175, 2016. https://doi.org/10.1109/JPROC.2015.2494218

[16] M. Irhouma, et al. “PID Controller Tuning for Electro Hydraulic Actuator using Radial Basis Function Neural Network,” *Wadi Alshatti University Journal of Pure and Applied Sciences*, vol. 3, no. 1, pp. 127–134, 2025. https://doi.org/10.63318/waujpasv3i1_19

[17] M. Mohamed, A. Yousef, and A. Hafez. “Concise Comparative Study of Economic Dispatch of Electrical Power Systems.” *Wadi Alshatti University Journal of Pure and Applied Sciences*, vol. 4, no. 1, pp. 404–413, 2026. https://doi.org/10.63318/waujpasv4i1_44

[18] D. Albuzia, A. Ali, M. Mohmed, and A. Hafez. “Reliable and Robust Optimal Interleaved Boost Converter Interfacing Photovoltaic Generator.” *Wadi Alshatti University Journal of Pure and Applied Sciences*, vol. 3, no. 2, pp. 192–201, 2025. https://doi.org/10.63318/waujpasv3i2_24

[19] L. Jiang, S. Tian, H. Huang, and H. Zhang. “Pseudoredundant Measurement-Based Adaptive Filtering for Estimation of Measurement Noise Covariance.” *IEEE Transactions on Instrumentation and Measurement*, vol. 75, Art. no. 3002516, 2026.https://doi.org/10.1109/TIM.2026.3699707